Contents lists available at SciOpen

Food Science and Human Wellness

journal homepage: https://www.sciopen.com/journal/2097-0765

China Food Publishing Co.

Naringenin nanoliposomes alleviate hyperuricemia by inhibiting NLRP3 inflammasome: effects of rigidity

Simin Feng[a,b], Jingjian Liu[a], Gaodan Liu[a], Jiahao Yu[a], Baihui Guo[a], Yihong Lan[c], Ping Shao[a,b,d,*]

[a] Department of Food Science and Engineering, Zhejiang University of Technology, Hangzhou 310014, China
[b] Key Laboratory of Food Macromolecular Resources Processing Technology Research (Zhejiang University of Technology), China National Light Industry, Hangzhou 310014, China
[c] Suntar Research, Singapore 638584, Singapore
[d] Moganshan Research Institute at Deqing County, Zhejiang University of Technology, Deqing 313211, China

ARTICLE INFO

Article history:
Received 10 September 2024
Received in revised form 14 October 2024
Accepted 7 November 2024

Keywords:
Nanoliposome
Rigidity
Naringenin
Hyperuricemia
Uric acid excretion
Inflammation

ABSTRACT

Hyperuricemia (HUA) is a metabolic disease characterized by high levels of uric acid (UA) in the blood and varying degrees of kidney damage. Desirable nanoliposomes should simultaneously exhibit efficient biocompatibility and effective drug delivery. However, they both usually require special structural properties. Herein, we propose a strategy to prepare nanoliposomes with varying rigidity by replacing cholesterol (CH) with phytosterol esters (PE). The results showed that the particle size of PE naringenin nanoliposomes (PE-NAR) was 179.5 nm, and the encapsulation efficiency (EE) was 79.93%. In atomic force microscopy (AFM) tests, PE-NAR showed a 1-fold increase in rigidity compared to CH naringenin nanoliposomes (CH-NAR). By observing the effects of naringenin nanoliposomes (NAR-NLs) on the physiological and biochemical indicators in HUA mice, we explore its impact on kidney damage and inflammatory pathways in HUA mice. The results show that NAR-NLs significantly inhibit UA levels and improve kidney damage. Compared to oral naringenin, NAR-NLs generally enhance the *in vivo* antioxidant effects of naringenin. Furthermore, high-rigidity PE-NAR downregulated the renal inflammatory factor interleukin-1β (IL-1β) to 6.67%, demonstrating the highest inhibitory effect. Further experiments have demonstrated that naringenin exerts a protective effect in kidney injury by inhibiting the activation of NOD-like receptor protein 3 (NLRP3) inflammasome and reducing oxidative stress within the body. In summary, by adjusting the rigidity of the nanoliposomes, the oral administration of naringenin can effectively improve the alleviation of HUA.

1. Introduction

Hyperuricemia (HUA), characterized as serum uric acid (UA) level exceeds 7 mg/dL, is a metabolic disease caused by abnormal purine metabolism or UA excretion in humans[1]. In recent years, due to abnormal dietary habits and lifestyles, such as overconsumption of high-purine food, the increasing prevalence of HUA in the population has become an unstoppable trend[2]. HUA has been found to be a contributing factor in the progression of gout and chronic kidney disease[3-4]. Furthermore, previous studies have confirmed a strong correlation between HUA and the incidence of insulin resistance, cardiovascular disease, hypertension, and diabetes[5]. UA is maintained in dynamic balance in healthy humans, with 600–700 mg of UA produced and excreted daily[6]. Excess UA in the blood stimulates the mesangial cells to generate a large amount of reactive oxygen species (ROS)[7]. Meanwhile, a high level of serum UA promotes the release of

* Corresponding author at: Department of Food Science and Engineering, Zhejiang University of Technology, Hangzhou 310014, China.
E-mail address: pingshao325@zjut.edu.cn (P. Shao)
Peer review under responsibility of Beijing Academy of Food Sciences.

SciOpen Publishing services by Tsinghua University Press

http://doi.org/10.26599/FSHW.2024.9250454

pro-inflammatory cytokines *via* the nuclear factor kappa-B (NF-κB) signaling pathway[8]. Hence, controlling serum UA levels and reducing kidney inflammation are considered two key strategies in terms of HUA treatment. Numerous anti-HUA drugs have been developed for HUA therapy, such as allopurinol, febuxostat, and benzbromarone[9]. However, the adverse reactions of these drugs, such as rashes, severe allergies, and nephrotoxicity, sometimes limit their clinical application[10]. Hence, safe and effective strategies against HUA are urgently needed to replace current drug therapies.

In recent years, more and more studies have focused on phytochemicals to regulate UA levels and prevent related diseases[11]. Naringenin, which is derived from citrus fruits, such as lemons and oranges, is a citrus flavonoid[12]. When used as a food supplement, naringenin might have various pharmacological activities *in vivo*, including antioxidant, antimicrobial, and suppressing inflammation activities[13-14]. In the study of HUA mice induced by potassium oxonate (PO) and fructose water, naringenin played a protective role in renal injury by inhibiting increases in the levels of proinflammatory cytokines interleukin-16 (IL-16) and tumor necrosis factor alpha (TNF-α)[15]. *In vitro*, naringenin has notable activities of inhibiting xanthine oxidase (XOD) and adenosine deaminase (ADA) to reduce urate production[16-17]. However, the low solubility of naringenin reduces its availability by hindering its transport across biological membranes[18]. This largely limits the application of naringenin in the pharmaceutical field.

Drug delivery systems involve delivering the potentially active drug to the site of action via a nano-vehicle to enhance the pharmacological properties of free drugs[19]. Nanoliposomes are one of the most explored nanocarriers used in targeted drug delivery systems. Nanoliposome is a kind of lipid bilayer colloidal vesicles with a nanometer size range, which can encapsulate compounds with poor water solubility[20]. However, the role of nanoliposomes is mainly affected by a variety of factors, including composition, particle size, surface charge, and biological environment[21]. Recently, studies have shown that nanoliposomes with greater rigidity exhibit favorable stability in simulated gastrointestinal tract experiments[22]. Our latest studies have shown that high-rigidity 1,2-dipalmitoyl-*sn*-glycero-3-phosphocholine (DPPC) nanoliposomes have the best endocytosis in cell uptake experiments[23]. Phytosterol, as a natural triterpenoid, plays a similar role as cholesterol (CH) in regulating the rigidity and membrane stability of nanoliposomes[24]. In addition, phytosterols have the health effects of reducing serum CH levels and preventing cardiovascular and cerebrovascular diseases[25]. Therefore, it is feasible to use phytosterols instead of CH to prepare nanoliposomes and regulate their rigidity.

In this study, phytosterol ester (PE) was used to replace CH to prepare nanoliposomes, and it was found that naringenin could be effectively encapsulated. The rigidity of nanoliposomes was obtained by atomic force microscopy (AFM) quantization to determine the feasibility of PE as membrane stabilizers instead of CH. Then, PO (200 mg/kg) and hypoxanthine (HX, 100 mg/kg) were used to induce a HUA model to observe the renal injury[26]. The therapeutic effects of different rigid naringenin nanoliposomes (NAR-NLs) on HUA mice were evaluated by further detecting UA, creatinine (Cr), blood urea nitrogen (BUN), malondialdehyde (MDA), superoxide dismutase (SOD), glutathione peroxidase (GSH-PX), and cytokine levels. Finally, the effect of NAR-NLs on the NOD-like receptor protein 3 (NLRP3) inflammasome was studied to elucidate its mechanism of improving renal inflammation.

2. Materials and methods

2.1 Materials and reagents

Naringenin were purchased from Shanghai Macklin Biochemical Co., Ltd. (Shanghai, China). DPPC and 1,2-dioleoyl-3-trimethylammoniumpropane (DOTAP) were obtained from AVT Pharmaceutical Co., Ltd. (Shanghai, China). PE were purchased from Xi'an Healthful Biotechnology Co., Ltd. (Xi'an, China). UA, Cr, BUN, XOD, MDA, SOD and GSH-PX texting kits were provided by Nanjing Key GEN Biotech. Co., Ltd. (Nanjing, China). Enzyme linked immunosorbent assay (ELISA) kit of IL-1β and 1L-18 was obtained from Cusabio Biological Engineering Co., Ltd. (Wuhan, China). All other materials used were of analytical grade.

2.2 Preparation of NAR-NLs

NAR-NLs were prepared by ethanol injection method[27]. Briefly, naringenin was dissolved in anhydrous ethanol and chloroform (V:V = 1:1) according to the ratio of DPPC:CH/PE: DOTAP = 0.65:0.25:0.1, and fully dissolved by ultrasound for 5 min. The organic phase was injected into a 5% glucose aqueous solution and an appropriate amount of Tween 80, and then the mixture was placed in a rotary evaporator and evaporated under reduced pressure at 45 ℃ for 30 min to remove the residual solvent. An appropriate amount of 5% glucose aqueous solution was used to obtain 10 mL liposome suspension.

2.3 Characterization of NAR-NLs

2.3.1 Particle size and zeta-potential measurements

A Zetasizer Nano ZS90 (Malvern Instruments Ltd., UK) was used to determine particle sizes, polydispersity indexes (PDI) and zeta potentials of the CH/PE-NAR. Before measurement, the CH/PE-NAR were diluted 4-fold with deionized water to prevent multiple scattering. Then, 1 mL of diluted sample was pipetted into the sample cell and tested at 25 ℃ in triplicate.

2.3.2 Encapsulation efficiency (EE) and loading amount (LA)

The NAR-NLs EE and LA were determined according to a previously described method, with some modification[23]. Briefly, 4 mL of NAR-NLs was centrifuged at 4 500 r/min for 15 min and then filtered through a 100 kDa membrane filter (Millipore) to separate free naringenin from the nanoliposomes. The concentration of free naringenin in the aqueous solution was determined by measuring the absorbance at 301 nm. The amount of free naringenin was determined using a standard curve (y = 0.003x + 0.014 2, R^2 = 0.995 3). EE and LA were calculated as follows:

$$\text{EE}\,(\%) = \frac{\text{Total NAR (mg)} - \text{Free NAR (mg)}}{\text{Total NAR (mg)}} \times 100 \quad (1)$$

$$\text{LA}\,(\text{g}/100\,\text{g}) = \frac{\text{Total NAR (g)} - \text{Free NAR (g)}}{\text{Total lipids (g)}} \quad (2)$$

2.3.3 Microstructure and morphology analysis

The amount of free naringenin was determined by microstructure and morphology analysis. The morphology of the nanoliposomes was

observed using an HT-7700 instrument (Hitachi, Japan). The samples were diluted to an appropriate concentration and dropped on a carbon coated copper mesh. The excess dispersion was then absorbed with a filter paper. Samples after drying were loaded into a sample holder for observation.

2.4 AFM measurements

AFM imaging and force measurements were performed using an atomic force microscope (Oxford Cypher ES) in tap mode in aqueous media at (26 ± 1) ℃. Before the measurement, a micro-cantilever (BL-AC40TS-C2) with a specified spring constant of 0.09 N/m and a tip curvature radius of 10 nm (Olympus, Tokyo, Japan) was immersed in the sample for 30 min to achieve thermal equilibrium. The scanning speed is set to 1 Hz, the stretching/contraction rate is 1.98 m/s, and the driving amplitude is 0.1–0.2 V. The obtained morphology image pixel is 256 × 256, and multiple force curves are obtained from nanoliposomes with a diameter of 150−250 nm. At least 100 times of force curve analysis was performed on each nanoliposome to obtain sufficient data for statistical analysis.

2.5 AFM data analysis

The Shell model was used to fit the force and liposome deformation curves to extract Young's modulus (E)[28]. The model is applied to the elastic region, and the penetration of the AFM tip to the sample should not exceed 10% of its diameter. Shell model uses the following relationship:

$$F = \frac{E4h^2}{R\sqrt{3(1-v^2)}}\delta \tag{3}$$

Where F represents the applied force (N), R represents the radius of curvature of the indented nanoliposomes, h represents the membrane thickness and δ represents indentation. The Poisson's ratio (v) is typically assumed to be 0.5 and the membrane thickness 4 nm.

When immobilized nanoliposomes were positioned, closer images were recorded (typically 2 μm × 2 μm or smaller), and sections were drawn across the images to survey the height H and base width W of individual nanoliposomes, thereby ignoring tip convolution effects. The formula for calculating the volume V of the adsorbed nanoliposome is:

$$V = \frac{\pi H}{6}\left(\frac{3}{4}W^2 + H^2\right) \tag{4}$$

Moreover, the mean diameter D of a sphere of equivalent volume was calculated as:

$$D = \sqrt[3]{\frac{6V}{\pi}} = H\sqrt[3]{\frac{3}{4}\frac{W^2}{H^2} + 1} \tag{5}$$

2.6 Animals and treatment

Male Kunming mice (18–22 g) were purchased from the Hangzhou Qizhen Experimental Animal Technology Co., Ltd. (Hangzhou, China) (SCXK(Zhe)2022-0005). Animals were acclimated for 1 week before the experiments. All animals were allowed to eat a standard diet and drink *ad libitum*, and adapted to the specific pathogen free (SPF) conditions at (22 ± 2) ℃, humidity (60 ± 5)% with a fixed 12 h artificial light period. The study was guided and approved by the Animal Ethics Committee of Zhejiang University of Technology Medicine (MGS20230711097). All mice were randomly divided into 6 groups (n = 7 per group): (G1) control group, (G2) model group, (G3) benzbromarone group (20 mg/kg), (G4) naringenin group (50 mg/kg), (G5) CH-NAR group (40 mg/kg), and (G6) PE-NAR group (40 mg/kg). PO (200 mg/kg) and HX (100 mg/kg) were dissolved in 0.5% sodium carboxymethyl cellulose solution, and mice were intraperitoneally injected with combined modeling drugs to induce HUA. Naringenin and benzbromarone were dissolved in 0.5% sodium carboxymethyl cellulose solution. After 1 h of modeling, the corresponding therapeutic drugs were intragastrically administered. The control mice were treated with 0.5% CMC-Na for 14 days. The body weight, diet and water intake of each mouse were recorded before the experiment every day. On day 15, mice were euthanized 1 h after the final administered dose; the blood samples and tissues of the liver and kidney were collected and stored at −80 ℃. The kidney index and liver index uses the following relationship:

$$\text{Kidney index}\,(\%) = \frac{\text{Weight of kidney (mg)}}{\text{Body weight (g)}} \times 100 \tag{6}$$

$$\text{Liver index}\,(\%) = \frac{\text{Weight of liver (mg)}}{\text{Body weight (g)}} \times 100 \tag{7}$$

2.7 Biochemical measurement

The levels of UA, Cr, BUN and XOD in the serum and XOD in the liver were detected by using commercial detection kits (Jiancheng Bioengineering Institute, China) according to the instructions of manufacturers.

2.8 Histological analysis

After the mice were sacrificed, some kidney tissues were collected from each group of mice, washed with saline solution and fixed in 4% paraformaldehyde. The tissue samples were dehydrated and embedded in paraffin, and evenly cut into 4 μm sections. After staining with hematoxylin and eosin (H&E), the histopathological changes of the kidney were observed under an optical microscope magnification. The kidney injury was scored according to the previous.

2.9 Antioxidant activity and cytokine levels

The activities of MDA, SOD and GSH-PX in the serum were detected by using commercial detection kit (Jiancheng Bioengineering Institute, China) and the protein concentration of kidney supernatant was detected by BCA kit. The levels of IL-1β and IL-18 in the serum and kidney were detected by ELISA kits. The detection method was performed according to the instructions of manufacturers.

2.10 Immunohistochemical staining

The paraffin embedded kidney sections were deparaffinized using xylene and dehydrated using graded concentrations of alcohol. Antigen retrieval was conducted by autoclaving at 120 ℃ for 15 min in citrate buffer (pH 6.0), and then sections were incubated with 3% hydrogen peroxide was used to inactivate the endogenous peroxidase. Then, sections were blocked with 10% horse serum. And they were incubated with IL-1β antibody (1:200, Proteintech, Wuhan, China) for overnight at 4 ℃. Then, the sections were incubated with HRP-conjugated secondary antibody (Bioss, Beijing, China) for 1 h at

room temperature. Subsequently, the sections were incubated with streptavidin HRP (Bioss, Beijing, China), results were obtained *via* fluorescence microscopy.

2.11 Western blotting analysis

The kidney tissue was homogenized in protein lysate (RIPA:5× cooktail:PMSF:phosphatase inhibitor = 100:2:1:1), lysed on ice for 30 min, and centrifuged at 12 000 × *g* at 4 ℃ for 15 min. Then the supernatant was collected and the protein concentration was detected by BCA protein assay kit. The sample protein and the sample buffer were mixed in a ratio of 4:1 and boiled for 10 min.

The protein samples were separated by 8%–10% SDS-PAGE gel electrophoresis and transferred to PVDF membrane. The PVDF membrane was blocked in 5% skim milk at room temperature for 1 h, and incubated with 1∶1 000 diluted anti-NLRP3, apoptosis-associated speck like protein containing a CARD (ASC), Caspase-1 and IL-1β (Servicebio, Wuhan, China) antibodies at 4 ℃ overnight. Then, after washing with TBS-Tween for 3 times, these membranes were incubated with the second antibody at room temperature for 1 h. Protein bands were exposed using a chemiluminescence (ECL) kit (Beyotime, Nanjing, China) and quantified by ImageJ software. All protein expression levels were normalized to the expression level of *β*-actin.

2.12 Gene expression

The TRIzol reagent (Invitrogen, USA) was used to isolate the total RNA from kidney tissues following the standard protocol and then the RNA was reversely transcribed into cDNA using the HiScript II Q RT SuperMix kit (Vazyme Biotech Co., Ltd., China). The cDNA was amplified by using the SYBR Green PCR Master Mix and specific primers in the CFX96 Real-Time PCR Detection system (Bio-Rad, USA) and these primers were listed in Table S1. The *β-actin* was used as the housekeeping gene. All target genes were normalized with *β-actin*.

2.13 Statistical analysis

Data is expressed as means ± SD and all data analysis were using SPSS version 26.0 software. Differences between groups were determined using analysis of variance (ANOVA). When the *F* ratios were significant, post hoc comparisons were made using the least significant difference (LSD) post hoc test. $P < 0.05$ was considered statistically significantly.

3. Results

3.1 Characteristics of NAR-NLs

As depicted in Fig. 1A, NAR-NLs consist of translucent, milky white suspensions exhibiting a light blue glow, characterized by their uniformity, stability, and non-stratification. Nanoliposomes synthesized using CH and PE exhibited varying zeta-potentials, where PE-NAR ((40.87 ± 0.97) mV) surpassed CH-NAR ((35.16 ± 0.02) mV) by significant difference ($P < 0.05$). Polydispersity frequently served as a measure for the distribution of particle diameters in colloidal systems. The particle diameter distribution was narrow when the value of PDI was small, and thus particles showed better uniformity in diameter[29]. The PDI of nanoliposomes was (0.208 ± 0.030) and (0.221 ± 0.020), respectively, suggesting that the particle size distribution was uniform (Fig. 1B).

The EE and LA are important parameters determining the amount of bioactive components that can be loaded into nanoliposomes. Fig. 1C shows the EE and LA values for the CH-NAR and PE-NAR. There were no significant differences in EE and LA of nanoliposomes, with EE ranging from (77.33 ± 4.55)% to (79.93 ± 2.74)% and LA ranging from (4.64 ± 0.27) g/100 g to (4.79 ± 0.16) g/100 g ($P > 0.05$). Wang et al.[30] formulated liposomes of naringenin, and the EE was 78.89%. After oral administration, the relative bioavailability increased by about 13.44-fold.

The optical microscopic images and particle size distributions of the CH/PE-NAR are shown in Figs. 1D and E. The nanoliposomes particle sizes of 2 groups were not significantly different, and the sizes were all

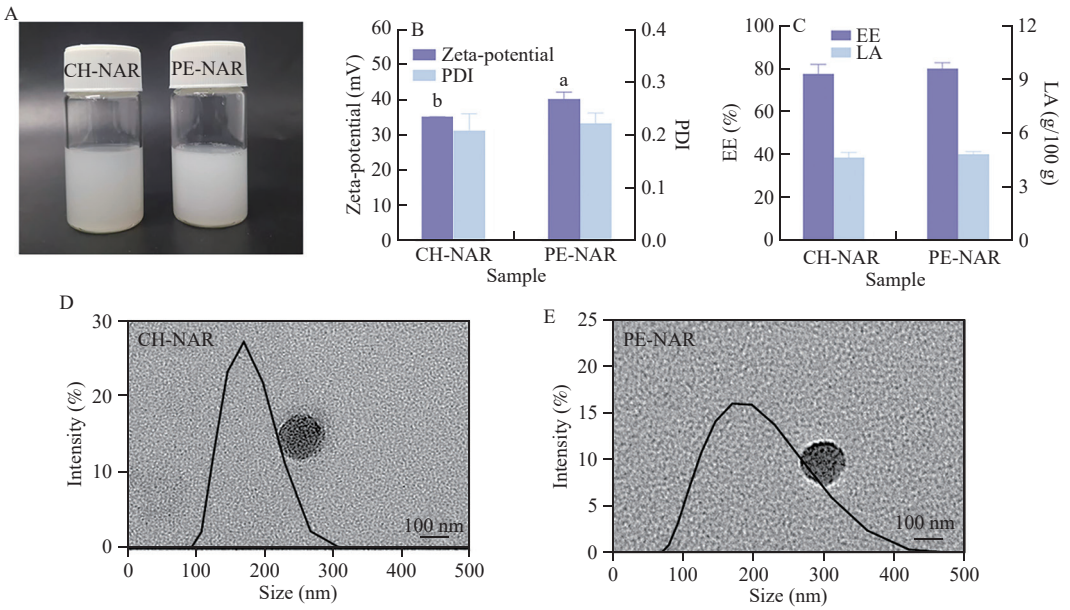

Fig. 1 Physicochemical characterization of NAR-NLs. (A) Appearance. (B) Zeta-potential and PDI. (C) EE and LA. Transmission electron microscope (TEM) and particle size distributions of (D) CH-NAR and (E) PE-NAR. Scale bar = 100 nm. Data are presented as the mean ± SD ($n = 3$), different letters indicate significant differences ($P < 0.05$).

in the range of (184.77 ± 1.46)−(179.50 ± 3.96) nm ($P > 0.05$). This was because the size heterogeneity was reduced after the nanoliposomes were extruded through the polycarbonate filters. The two nanoparticles have similar spherical structures and smooth surfaces.

3.2 Study on the morphology and stiffness of NAR-NLs by AFM

We prepared 2 nanoliposome samples containing naringenin, adsorbed NAR-NLs on silicon wafers, and observed their morphology using AFM. Fig. 2A shows multiple dispersed circular particles without aggregation. Then, the width and new appearance of NAR-NLs were further observed by AFM. As shown in Fig. 2B, NAR-NLs exhibit a typical spherical shape with a width range of 193–235 nm. The diameter of nanoliposomes measured by AFM was larger than the average diameter measured by the particle size analyzer and TEM. The volume and average diameter of the equivalent sphere were calculated using Equations (4) and (5), and the average particle size measured by the particle size analyzer was compared (Table S2). The results showed that the average diameters of CH-NAR ((179.61 ± 4.08) nm) and PE-NAR ((176.96 ± 5.38) nm) were not significantly different from those measured by particle size analyzer.

While imaging the NAR-NLs surface, multiple scans were performed to obtain the corresponding force-deformation curve. The set point of more than 2 nN gives the jump state of the force-deformation curve, indicating that the AFM tip will produce sharp indentations, thereby penetrating the lipid membrane. In order to avoid plastic deformation, the maximum force of the set point is less than 500 pN. In addition, nanoliposomes with a height greater than 35 nm were selected to analyze their stiffness to avoid being affected by the substrate. The experiment only collected the elastic behavior data of NAR-NLs with less deformation, that is, the maximum indentation is about 10% of the measured liposome height. The force-deformation curves of CH-NAR and PE-NAR are shown in Fig. 2C. Compared with CH-NAR, the force-deformation curve obtained by PE-NAR is steeper. The stiffness of CH-NAR and PE-NAR obtained by linear curve fitting is shown in Fig. 2D, which are (19.88 ± 1.35) and (45.05 ± 3.55) pN/nm, respectively. The nanoliposome with the larger Young's modulus was determined to be PE-NAR by Shell model, reaching (93.42 ± 7.37) MPa, which was significantly higher than that of CH-NAR ((41.86 ± 2.85) MPa).

3.3 Effects of naringenin on HUA function in mice

To evaluate the impact of naringenin on HUA, a mice model of HUA was established (Fig. 3A). The body weight of mice in G2 began to decrease on the 7th day, and decreased to (31.0 ± 0.5) g on the fourteenth day, which was significantly lower than that in G1 ($P < 0.05$). Benzbromarone and varied doses of naringenin effectively reversed this outcome, resulting in a steady gain in body weight, ranging from (36.6 ± 2.8) g to (38.3 ± 0.4) g over time (Fig. 3B). G2 consumed (2.5 ± 0.2) g of food, significantly less than G1 ((6.5 ± 0.2) g; $P < 0.01$). Other treatment groups alleviated this occurrence (Fig. 3C). However, different treatment strategies had no effect on the drinking water intake of either group ($P > 0.05$; Fig. 3D).

3.4 Naringenin reduced UA levels in HUA mice

As shown in Fig. 4A, the serum UA level in G2 were significantly increased to 244.53 μmol/L compared to G1 (79.47 μmol/L) ($P < 0.05$).

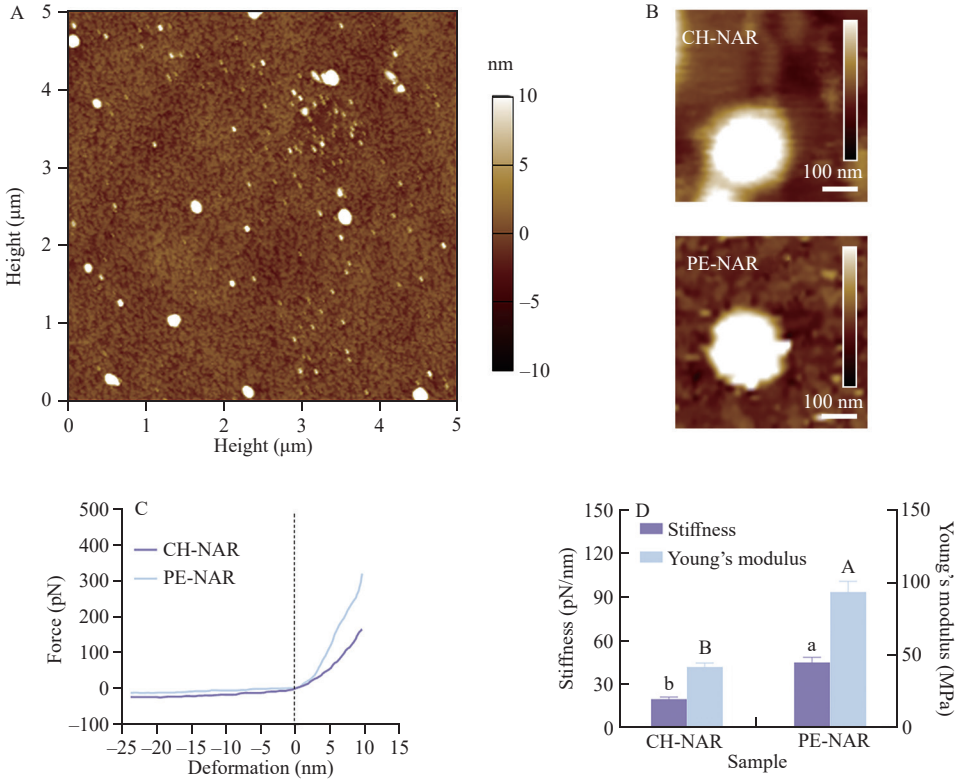

Fig. 2 AFM measurements of NAR-NLs. (A) Typical AFM two-dimensional images of CH-NAR. (B) The AFM morphologies of CH-NAR and PE-NAR. (C) Force-deformation curve obtained from NAR-NLs. (D) Stiffness and Young's modulus of NAR-NLs. Scale bar = 100 nm. Data are presented as the mean ± SD ($n = 5$), different letters for the same index indicate significant differences ($P < 0.05$).

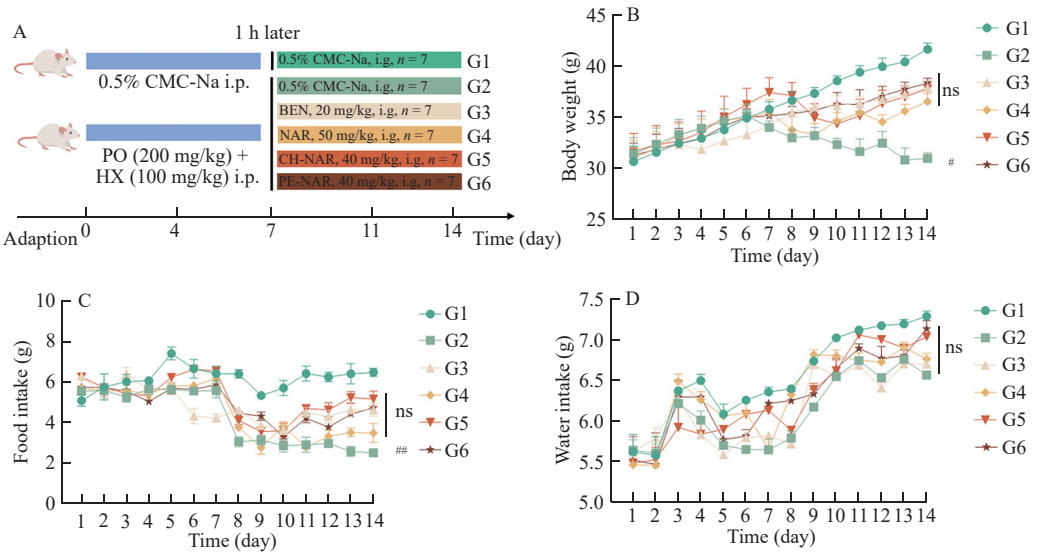

Fig. 3 Effects of naringenin on mice with HUA. (A) Schematic diagram of animal experiment design. BEN, benzbromarone; NAR, naringenin. (B) Body weight. (C) Food intake. (D) Water intake. All the results are shown as mean ± SD ($n = 7$). $^{\#}P < 0.05$ and $^{\#\#}P < 0.01$ *vs*. G2, and ns means no significant difference ($P > 0.05$).

Serum UA in G6 was considerably lowered to 112.12 μmol/L ($P < 0.05$). G4 and G5 significantly lowered serum UA levels to 184.69 and 166.10 μmol/L ($P < 0.05$), respectively. Furthermore, G3 showed significantly greater serum BUN levels than G1 ($P < 0.05$). In HUA mice, naringenin and NAR-NLs significantly lowered serum BUN levels ($P < 0.05$; Fig. 4B). Compared to G1 (56.13 μmol/L), serum Cr in G2 increased dramatically to 86.79 μmol/L. Both 20 mg/kg benzbromarone and 40 mg/kg NAR-NLs significantly reduced serum Cr levels to 57.56 and 63.21 μmol/L, respectively ($P < 0.05$; Fig. 4C).

In addition, serum levels of MDA, SOD and GSH-PX were examined (Figs. 4D-F). In comparison to G1, serum MDA levels in G2 increased dramatically to 12.40 nmol/mL ($P < 0.05$), while serum SOD and GSH-PX levels decreased significantly ($P < 0.05$). However, treatment of CH-NAR and PE-NAR groups downregulated MDA levels ($P < 0.05$) and dramatically elevated SOD and GSH-PX levels ($P < 0.05$), indicating that CH-NAR and PE-NAR can reduce oxidative stress in HUA mice.

3.5 Naringenin ameliorated PO/HX-induced kidney histopathological injuries

The inflammatory cell infiltration and tissue damage are considered pathological features of HUA[31]. As shown in Fig. 5A, the outer appearance of mice kidneys from G1 revealed a reddish color. However, the kidneys in G2 and G3 appeared pale and edematous. The treatment with naringenin can restore the ruddy smooth phenomenon. In addition, the treatment of naringenin reduced the kidney index to 1.96%–1.75% (Fig. 5C), respectively. Consistent with

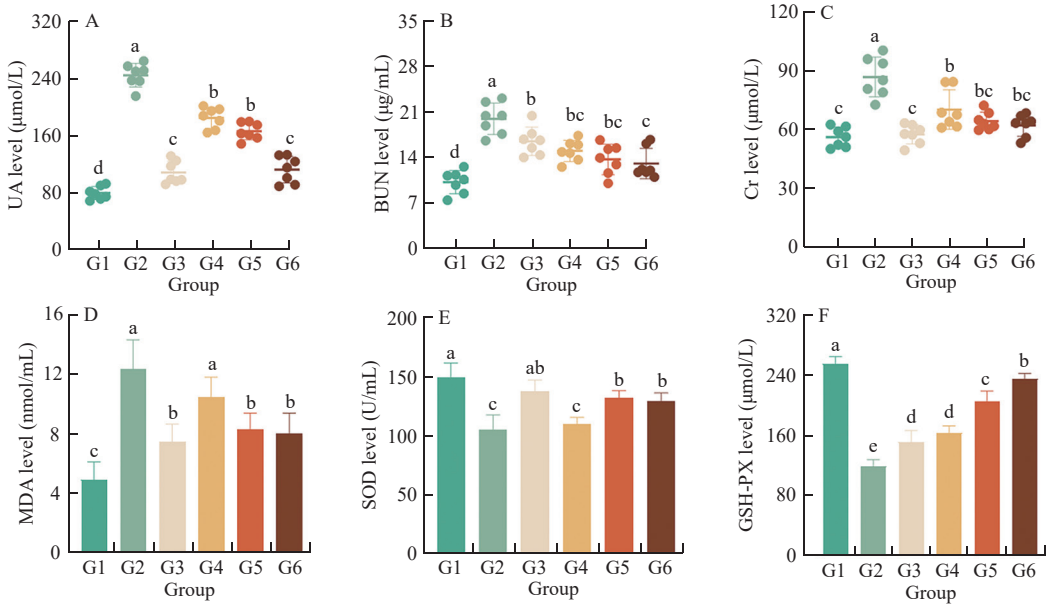

Fig. 4 Effects of naringenin on biochemical indexes of HUA mice. (A) UA level. (B) BUN level. (C) Cr level. (D) MDA level. (E) SOD level. (F) GSH-PX level. Data are presented as the mean ± SD ($n = 7$), different letters indicate significant differences ($P < 0.05$).

these results, H&E staining demonstrated (Fig. 5B) that the kidney tissue morphology of mice in G1 was normal and there was no sign of inflammation. While the kidney tissues in G2 displayed serious kidney histopathological injuries, characterized by atrophic glomeruli and unusual tubular structure. However, G6 remarkably prevented the damage to the glomeruli and tubules, with intact glomeruli and regular tubules being observed. Compared with G2 (3.94), the histopathological score of G6 was significantly decreased to 1.06 ($P < 0.05$; Fig. 5D). Overall, these findings indicated that naringenin could effectively alleviate kidney damage in the case of HUA.

3.6 *Naringenin decreased the levels of XOD in serum and liver*

XOD is highly expressed in the liver and is the critical enzyme functioning for catalyzing the transformation of HX into xanthine and then to UA[32]. Therefore, the effects of naringenin on the activities of XOD in serum and liver were investigated to explore the mechanism of lowering serum UA levels *via* the UA synthesis pathway. As shown in Figs. 6A and B, G2 had a significantly higher XOD level in serum and liver as compared to those levels in G1 ($P < 0.05$). Compared with G2 (44.93 U/L), G3 or G6 treatment significantly reduced serum XOD levels to 32.64 and 33.33 U/L, respectively ($P < 0.05$). In addition, XOD levels in the liver also showed the same reversal trend. Benzbromarone administration could trigger liver injury in mice[33]. In order to evaluate the potential hepatotoxicity of the test articles in HUA mice, liver index, serum aspartate aminotransferase (AST), alanine transaminase (ALT) and liver ALT and AST levels were measured. As shown in Fig. 6C, no noticeable changes were observed in liver index among the groups ($P > 0.05$). As shown in Figs. 6D and E, G2 had higher serum ALT and AST levels than G1 ($P < 0.05$). G5 and G6 significantly reduced serum ALT and AST levels in HUA mice, and the reversal effect of G6 was more significant. Compared with G2, 20 mg/kg benzbromarone treatment (G3) did not improve serum ALT and AST levels ($P > 0.05$). The average serum ALT and AST in G3 were 18.38 and 18.78 U/L, respectively. Besides, in the liver, no differences among the groups in the AST and ALT levels were observed ($P > 0.05$; Figs. 6F and G).

3.7 *Naringenin inhibited the production of cytokines in serum and kidney tissues in HUA mice*

To assess the degree of kidney inflammation, we further investigated the levels of inflammatory cytokines IL-1β and IL-18 in serum and kidney tissue HUA mice. Compared with G1, the levels of IL-1β and IL-18 in serum and kidney of HUA mice (G2) were significantly upregulated ($P < 0.05$; Figs. 7A-D). Compared with G2, 40 mg/kg of G5 and G6 reversed this level for 2 weeks. Of note, compared with G5, the G6 significantly inhibited the expression of inflammatory cytokines, including serum IL-1β, IL-18, and kidney IL-18 ($P < 0.05$). However, the G4 had no significant effect on renal IL-1β and IL-18 levels ($P > 0.05$). Furthermore, the immunohistochemical examination of renal IL-1β revealed a notable rise in IL-1β positive staining in mice with HUA (Fig. 7E). Compared with G2 (33.67%), the quantitative analysis of renal IL-1β immunohistochemical staining in G5 and G6 was significantly downregulated to 11.33% and 6.67% ($P < 0.05$; Fig. 7F). There was no significant difference between G6 and G1 (5.33%). The findings indicate that by integrating naringenin into phytosterol nanoliposomes, it's more effective in suppressing inflammatory cytokines' expression, thus lessening renal inflammation in mice with HUA.

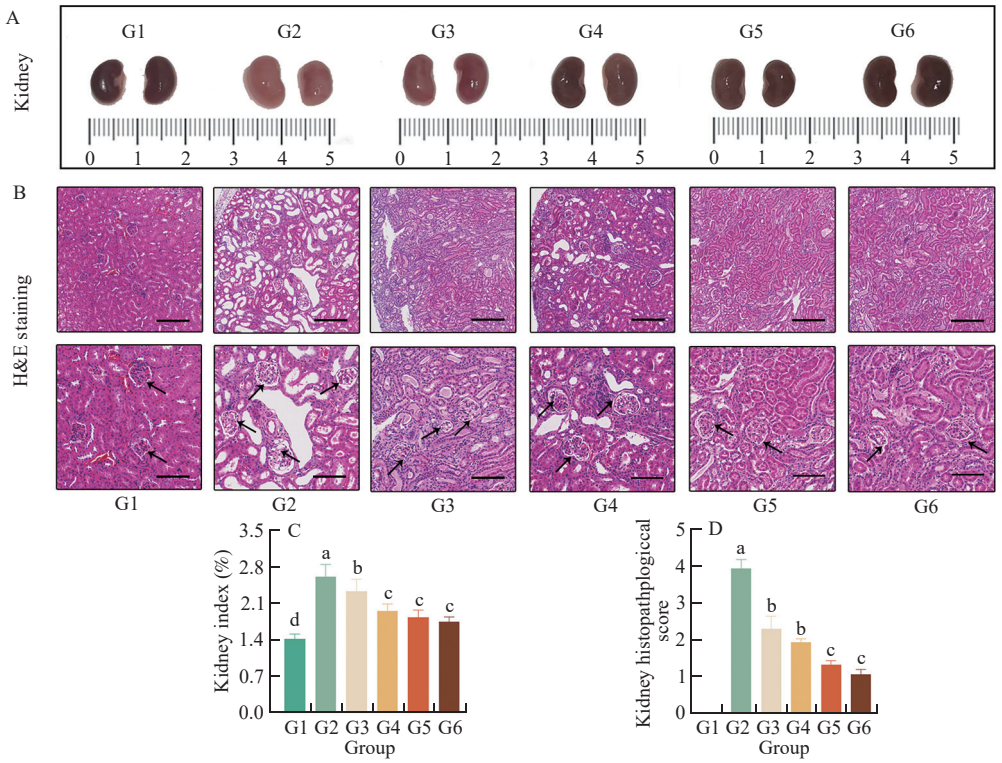

Fig. 5 Effects of naringenin on pathological changes of kidney tissues in HUA mice. (A) Kidney surfaces. (B) Kidney H&E-stained sections with magnification. Black arrows represent glomeruli. (C) Kidney index. (D) Kidney histopathology score. Scale bar = 200 μm (top) and 100 μm (bottom). Data are presented as the mean ± SD ($n = 3$), different letters indicate significant differences ($P < 0.05$).

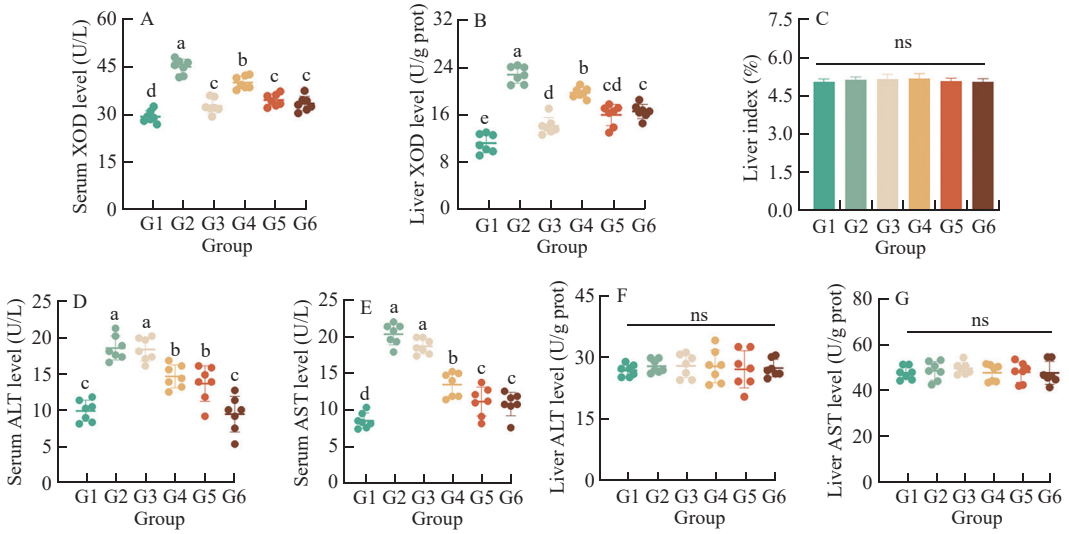

Fig. 6 Effects of naringenin on liver excretion in HUA mice. (A) Serum XOD level. (B) Liver XOD level. (C) Liver index. (D) Serum ALT level. (E) Serum AST level. (F) Liver ALT level. (G) Liver AST level. Data are presented as the mean ± SD (n = 7), different letters indicate significant differences (P < 0.05), and ns means no significant difference (P > 0.05).

3.8 Naringenin suppress NLRP3 inflammasome activation to inhibit kidney inflammation

As a downstream factor of the NLRP3 inflammasome, IL-1β plays a key role in the NLRP3 signaling pathway[34]. On this basis, we further studied the effect of naringenin on the NLRP3 inflammasome signaling pathway. Compared with G1, the mRNA expression of *NLRP3*, *ASC*, *Caspase-1* and *IL-1β* in the kidney tissues of mice with HUA (G2) induced by PO and HX was significantly increased (P < 0.05). In addition, different doses of naringenin treatment groups could downregulate their mRNA levels. Among them, the mRNA expression of *Caspase-1* and *IL-1β* in 40 mg/kg G5 and G6 was significantly lower than that in G4 (P < 0.05; Figs. 8A-D). Next, the levels of NLRP3 inflammasome and downstream inflammatory

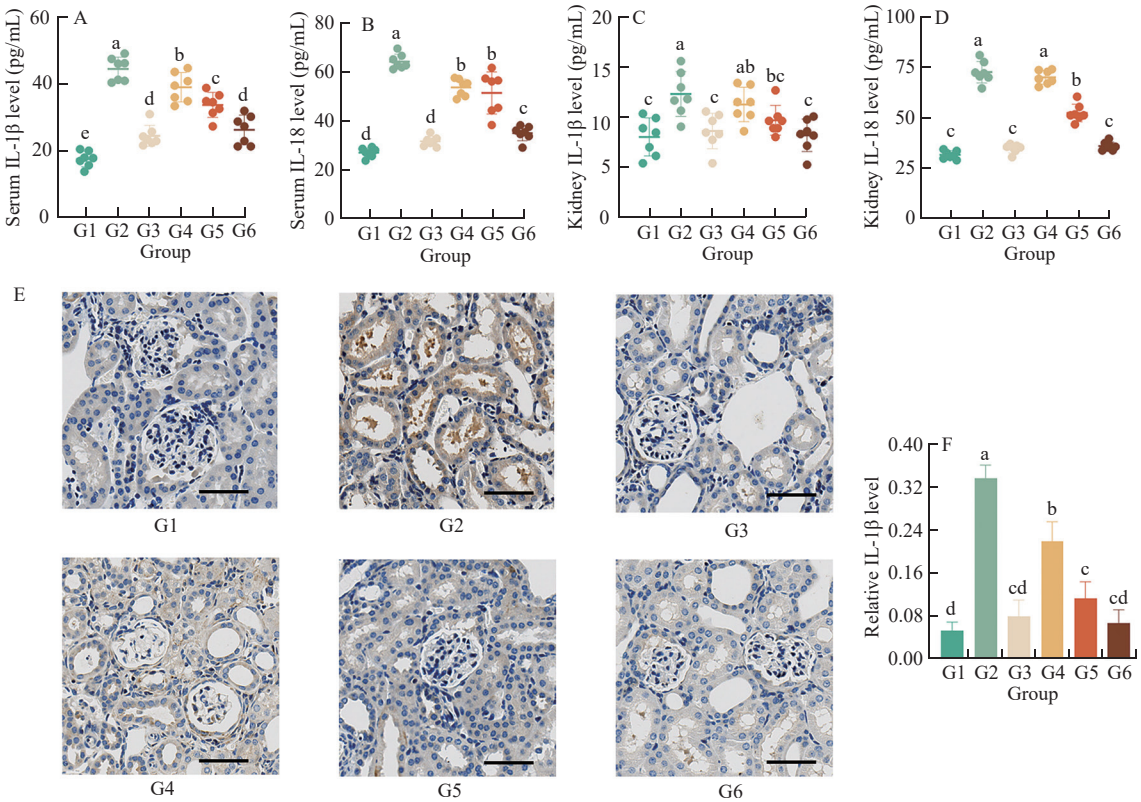

Fig. 7 Effects of naringenin on the levels of pro-inflammatory cytokines. (A) The level of IL-1β in serum. (B) The level of IL-18 in serum. (C) The level of IL-1β in kidney. (D) The level of IL-18 in kidney (n = 7). (E) The representative immunohistochemistry (IHC) pictures of IL-1β in kidney. Scale bar = 50 μm. (F) Quantitative analysis of IHC staining (n = 3). All the results are shown as mean ± SD, different letters indicate significant differences (P < 0.05).

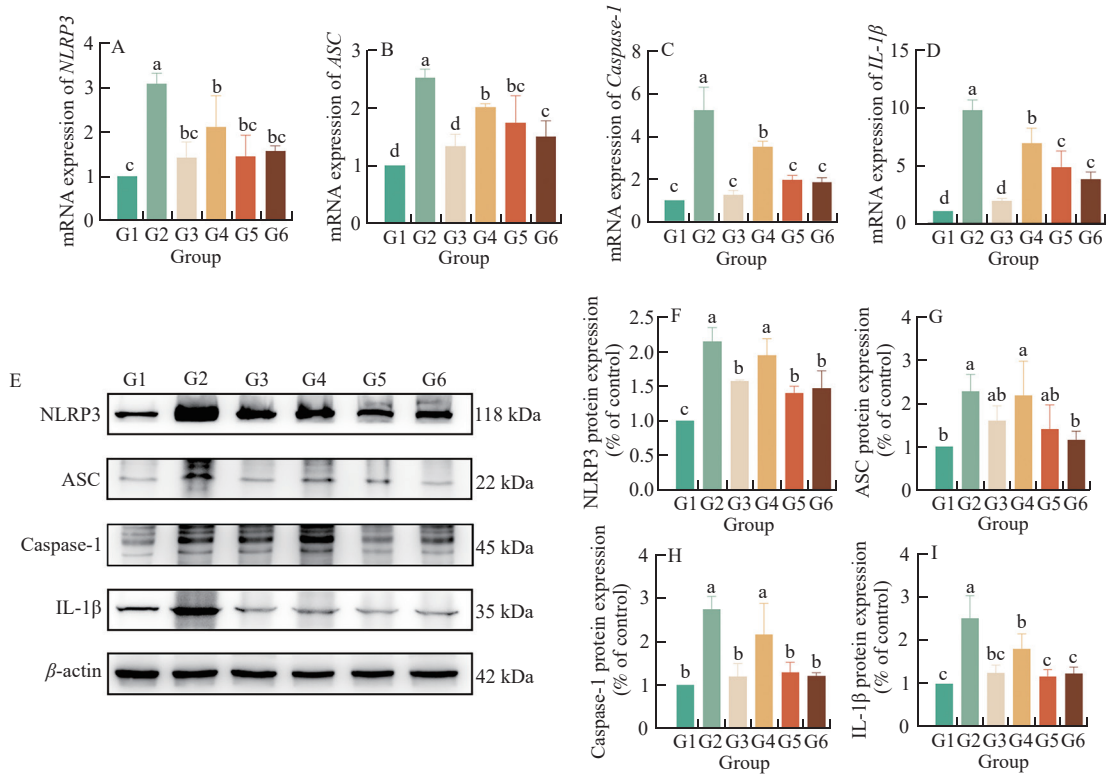

Fig. 8 Naringenin suppressed NLRP3 inflammasome activation. mRNA expression levels of (A) *NLRP3*, (B) *ASC*, (C) *Caspase-1*, and (D) *IL-1β* ($n = 3$). (E) Representative Western blots of NLRP3, ASC, Caspase-1, and IL-1β protein expression. Quantitative analysis of (F) NLRP3, (G) ASC, (H) Caspase-1, and (I) IL-1β protein expression ($n = 3$). All the results are shown as mean ± SD, different letters indicate significant differences ($P < 0.05$).

cytokines in the kidney were evaluated by Western blotting (Fig. 8E). The expression of NLRP3, ASC, and Caspase-1 in G2 was significantly increased, and the expression of related downstream inflammatory cytokines IL-1β was increased ($P < 0.05$). G6 inhibited the expression of NLRP3, ASC, and Caspase-1, and inhibited the expression of the pro-inflammatory cytokine IL-1β ($P < 0.05$; Figs. 8F-I). In contrast, G5 administration did not significantly inhibit the expression of ASC ($P > 0.05$; Fig. 8G). It is worth noting that the 50 mg/kg G4 had little effect on inhibiting the NLRP3 inflammasome, because it only inhibited the protein expression of downstream inflammatory cytokine IL-1β ($P < 0.05$; Fig. 8I).

4. Discussion

Nanoliposomes are an important way to overcome the intestinal barrier and enhance the solubility, stability, and bioavailability of sensitive bioactive ingredients[35-36]. The size and potential of nanoliposomes play a key role in the digestion, release, and absorption of encapsulated drugs[37]. Similarly, the rigidity of the nanoliposomes affects their stability, the release profile of the loaded drug, and the effectiveness of drug delivery[28]. Phytosterols play an important role in controlling membrane fluidity and permeability, and their own molecular structure will influence the rigidity of liposomes constructed by them[24]. Studies with model membrane systems have shown that phytosterol molecules have three properties that enable them to embed in the phospholipid bilayer[38]. By restricting the movement of the acyl chains of the phospholipid bilayer acyl chain and anchoring the choline ammonium group close to the membrane surface, it leads to an increase in membrane ordering and rigidity of the nanoliposomes[24]. For NAR-NLs, the incorporation of PE resulted in a significantly greater rigidity of the nanoliposomes than that of CH nanoliposomes. Among them, the Young's modulus of PE-NAR calculated by the Shell model is (93.42 ± 7.37) MPa (Figs. 2C, D). This was attributed to the fact that the ester carbonyl group of PE could form hydrogen bonds with the polar head group (PO^{2-}) of the phospholipid, leading to changes in the stacking geometry of the phospholipid bilayer and increased membrane cohesion, thereby enhancing the stability of the bilayer[39].

The efficient utilization of bioactive compounds is important for precision nutrition in disease prevention[40]. Advances in nanotechnology have made nanoliposomes a promising vehicle for delivering natural active ingredients to improve their oral bioavailability. Chen et al.[41] prepared nanoliposomes with an inhibitory effect on NAFLD comparable to that of the original naringenin, but at a dose fourfold lower than that of the original drug. In our study, 50 mg/kg of naringenin treatment group did not reverse serum oxidative indices in HUA mice. On the contrary, 40 mg/kg of NAR-NLs significantly improved this parameter (Figs. 4D-F). The encapsulation of nanoliposomes resulted in enhanced solubility of naringenin. After administration, the PE-NAR significantly reduced serum AST and ALT levels (Figs. 6D, E). The positive control benzbromarone group (20 mg/kg) showed some side effects in the treatment of HUA mice, and the high expression of serum AST and ALT can indicate this. As a novel, natural, and safe phytochemical, naringenin can be used as an auxiliary preparation against HUA to reduce some side effects. Jiang et al.[42] demonstrated that naringenin restores c-fos expression and promotes flap viability by reducing oxidative stress and apoptosis. The modulation of stiffness resulted in enhanced diffusivity of the nano-lipid particles through the epithelium for more effective

drug delivery[43]. In addition, the ability to overcome the epithelial barrier could be improved by modulating the stiffness of the amphiphilic ionic hydrogel nanoparticles, where the more rigid nanoparticles exhibit overall higher transport efficiency[44]. This effect was reflected in the ability of PE to significantly reduce the oxidative stress of the inflammatory factors IL-1β and IL-18 naringenin.

XOD is a key enzyme involved in the conversion of xanthine and HX to UA, and its activity has an important effect on UA production[45]. Studies have shown that a large number of flavonoids have notable activities of inhibiting XOD and ADA to reduce urate production and reverse urate excretion and reabsorption by regulating renal urate transporters glucose transporter 9 (GLUT9), adenosine triphosphate (ATP) -binding cassette efflux transporter G2 (ABCG2) and organic anion transporter 1 (OAT1) [11]. The results showed that naringenin blocked serum UA production in HUA mice by inhibiting XOD activity (Figs. 6A, B). The excessive accumulation of UA will show cytotoxic effects, and the pathological effects include inducing renal interstitial inflammatory injury[46]. In addition, oxidative stress and pro-inflammatory cytokines are crosstalk in the induction of HUA[47]. These factors activate the NLRP3 inflammasome, promote the secretion of pro-inflammatory factors by inflammatory cells, up-regulate the level of inflammation in the kidney, and cause inflammatory damage in the kidney[48]. NLRP3 inflammasome is formed by oligomerization of pattern recognition receptor 3 with apoptosis-associated speck-like protein (ASC) and Caspase-1 precursor[49]. Under normal physiological conditions, Pro-caspase1 is inactive. When the NLRP3 inflammasome is activated, Pro-caspase-1 is processed and activated into active Caspase-1, and then the IL-1β precursor and IL-18 precursor are cleaved to generate and release IL-1β and IL-18, which is involved in the pathogenesis of various inflammatory diseases[50]. In this study, naringenin inhibited oxidative stress induced by PO combined with HX by increasing the levels of endogenous antioxidants GSH-PX and SOD. In addition, the pro-inflammatory cytokines IL-1β and IL-18 in the serum and kidney of HUA mice were significantly increased, indicating that the NLRP3 inflammasome was activated and inflammatory factors were produced to increase the inflammatory damage to the kidney. After NAR-NLs intervention, the levels of IL-1β and IL-18 in serum and kidney of HUA mice were down-regulated, and the expression of the NLRP3, IL-1β, and Caspase-1 proteins in kidney was decreased. It indicates that the activation of the NLRP3 inflammasome is inhibited, the level of renal inflammation is reduced, and renal injury is improved.

5. Conclusion

In conclusion, PE can be utilized as stabilizers to regulate the rigidity of nanoliposomes, and naringenin embedding allows for HUA. AFM was used to measure the rigidity of the nanoliposomes and evaluate its impact on naringenin bioavailability. The results demonstrated that PE-NAR has a high encapsulation rate and stiffness. *In vivo* investigations revealed that rigid nanoliposomes containing naringenin were effective at decreasing UA levels in HUA mice. Rigid nanoliposomes reduced oxidative stress more effectively than flexible nanoliposomes. Further research found that NAR-NLs alleviated kidney damage in HUA mice by suppressing NLRP3 inflammatory vesicles. Rigidly modifying nanoliposomes to behave as natural active products is a promising method that might also be used to overcome some physiological barriers. More studies will be conducted in the future to study the effects of physiological barriers based on this stiffness in order to develop a more complete theoretical model.

Conflict of interest

Ping Shao is an editorial board member for *Food Science and Human Wellness* and was not involved in the editorial review or the decision to publish this article. The authors declare no conflict of interest.

Acknowledgements

This work was funded by National Key R&D Plan of China (2024YFE0109500), the National Natural Science Foundation of China (32472367, 32372249), and Key Program of the Natural Science Foundation of Zhejiang Province (HZSZ25C200001).

Appendix A. Supplementary information

Supplementary data associated with this article can be found, in the online version, at http://doi.org/10.26599/FSHW.2024.9250454.

References

[1] I.Y. Kim, K.D. Han, D.H. Kim, et al., Women with metabolic syndrome and general obesity are at a higher risk for significant hyperuricemia compared to men, J. Clin. Med. 8 (2019) 837. https://doi.org/10.3390/jcm8060837.

[2] R. Liu, C. Han, D. Wu, et al., Prevalence of hyperuricemia and gout in mainland China from 2000 to 2014: a systematic review and meta-analysis, International BR. 2015 (2015) 1-12. https://doi.org/10.1155/2015/762820.

[3] E. Russo, F. Viazzi, R. Pontremoli, et al., Association of uric acid with kidney function and albuminuria: the Uric Acid Right for heArt Health (URRAH) Project, J. Nephrol. 35 (2022) 211-221.

[4] K. Hahn, M. Kanbay, M.A. Lanaspa, et al., Serum uric acid and acute kidney injury: a mini review, J. Adv. Res. 8 (2017) 529-536. https://doi.org/10.1016/j.jare.2016.09.006.

[5] L. Yang, Q. Wei, Y. Sun, et al., Hyperuricemia and coronary heart disease: the mediating role of blood pressure and thrombospondin 3, Nutrition, Metabolism and Cardiovascular Diseases 33 (2023) 1969-1980. https://doi.org/10.1016/j.numecd.2023.06.001.

[6] M. Bian, J. Wang, Y. Wang, et al., Chicory ameliorates hyperuricemia via modulating gut microbiota and alleviating LPS/TLR4 axis in quail, Biomed. Pharmacother. 131 (2020) 110719. https://doi.org/10.1016/j.biopha.2020.110719.

[7] D. Cui, S. Liu, M. Tang, et al., Phloretin ameliorates hyperuricemia-induced chronic renal dysfunction through inhibiting NLRP3 inflammasome and uric acid reabsorption, Phytomedicine 66 (2020) 153111. https://doi.org/10.1016/j.phymed.2019.153111.

[8] L. Chen, Z. Lan, Polydatin attenuates potassium oxonate-induced hyperuricemia and kidney inflammation by inhibiting NF-κB/NLRP3 inflammasome activation via the AMPK/SIRT1 pathway, Food Funct. 8 (2017) 1785-1792. https://doi.org/10.1039/C6FO01561A.

[9] A. Mehmood, L. Zhao, C. Wang, et al., Management of hyperuricemia through dietary polyphenols as a natural medicament: a comprehensive review, Crit. Rev. Food Sci. Nutr. 59 (2019) 1433-1455. https://doi.org/10.1080/10408398.2017.1412939.

[10] N. Dalbeth, A.L. Gosling, A. Gaffo, et al., Gout, The Lancet 397 (2021) 1843-1855. https://doi.org/10.1016/S0140-6736(21)00569-9.

[11] S. Feng, S. Wu, F. Xie, et al., Natural compounds lower uric acid levels and hyperuricemia: molecular mechanisms and prospective, Trends Food Sci. Technol. 123 (2022) 87-102. https://doi.org/10.1016/j.tifs.2022.03.002.

[12] M. Sui, S. Feng, J. Yu, et al., Removal and recovery of deep eutectic solvent with membrane-based methodology: a promising strategy to

enhance extraction and purification of *Dendrobium officinale* flavonoids, Ind. Crop. Prod. 206 (2023) 117638. https://doi.org/10.1016/j.indcrop.2023.117638.

[13] Q. Wang, Y. Ou, G. Hu, et al., Naringenin attenuates non-alcoholic fatty liver disease by down-regulating the NLRP3/NF-κB pathway in mice, Br. J. Pharmacol. 177 (2020) 1806-1821. https://doi.org/10.1111/bph.14938.

[14] K. Uçar, Z. Göktaş, Biological activities of naringenin: a narrative review based on *in vitro* and *in vivo* studies, Nutr. Res. 119 (2023) 43-55. https://doi.org/10.1016/j.nutres.2023.08.006.

[15] B. Yang, M. Xin, S. Liang, et al., Naringenin ameliorates hyperuricemia by regulating renal uric acid excretion *via* the PI3K/AKT signaling pathway and renal inflammation through the NF-κB signaling pathway, J. Agric. Food Chem. 71 (2023) 1434-1446. https://doi.org/10.1021/acs.jafc.2c01513.

[16] C. Liu, H. Zhou, R. Zhang, et al., Anti-hyperuricemic and nephroprotective effect of geniposide in chronic hyperuricemia mice, J. Funct. Foods 61 (2019) 103355. https://doi.org/10.1016/j.jff.2019.05.011.

[17] K. Liu, W. Wang, B.H. Guo, et al., Chemical evidence for potent xanthine oxidase inhibitory activity of ethyl acetate extract of *Citrus aurantium* L. dried immature fruits, Molecules 21 (2016) 302. https://doi.org/10.3390/molecules21030302.

[18] J. Cai, H. Wen, H. Zhou, et al., Naringenin: a flavanone with anti-inflammatory and anti-infective properties, Biomed. Pharmacother. 164 (2023) 114990. https://doi.org/10.1016/j.biopha.2023.114990.

[19] T.M. Allen, P.R. Cullis, Drug delivery systems: entering the mainstream, Science 303 (2004) 1818-1822. https://doi.org/10.1126/science.1095833.

[20] S. Khorasani, M. Danaei, M.R. Mozafari, Nanoliposome technology for the food and nutraceutical industries, Trends Food Sci. Technol. 79 (2018) 106-115. https://doi.org/10.1016/j.tifs.2018.07.009.

[21] H. Nsairat, D. Khater, U. Sayed, et al., Liposomes: structure, composition, types, and clinical applications, Heliyon 8 (2022) e09394. https://doi.org/10.1016/j.heliyon.2022.e09394.

[22] M. Frenzel, A. Steffen-Heins, Whey protein coating increases bilayer rigidity and stability of liposomes in food-like matrices, Food Chem. 173 (2015) 1090-1099. https://doi.org/10.1016/j.foodchem.2014.10.076.

[23] G. Liu, P. Sun, J. Yan, et al., Regulation of nanoliposome rigidity and bioavailability of oligomeric proanthocyanidin with phytosterols containing different C3 branches, ACS Appl. Mater. Interfaces 15 (2023) 43414-43430. https://doi.org/10.1021/acsami.3c07854.

[24] C. Silva, F.J. Aranda, A. Ortiz, et al., Molecular aspects of the interaction between plants sterols and DPPC bilayers: an experimental and theoretical approach, J. Colloid Interface Sci. 358 (2011) 192-201. https://doi.org/10.1016/j.jcis.2011.02.048.

[25] Y. Wang, B. Liu, Y. Hu, et al., Phytosterol intake and risk of coronary artery disease: results from 3 prospective cohort studies, Am. J. Clin. Nutr. 119 (2024) 344-353. https://doi.org/10.1016/j.ajcnut.2023.11.020.

[26] J. Zhuang, X. Zhou, T. Liu, et al., Astaxanthin attenuated hyperuricemia and kidney inflammation by inhibiting uric acid synthesis and the NF-κB/NLRP3 signaling pathways in potassium oxonate and hypoxanthine-induced hyperuricemia mice, Pharmazie 76 (2021) 551-558. https://doi.org/10.1691/ph.2021.1731.

[27] A.A. Khafoor, A.S. Karim, S.M. Sajadi, Recent progress in synthesis of nano based liposomal drug delivery systems: a glance to their medicinal applications, Results in Surfaces and Interfaces 11 (2023) 100124. https://doi.org/10.1016/j.rsurfi.2023.100124.

[28] J. Eid, H. Greige-Gerges, L. Monticelli, et al., Elastic moduli of lipid membranes: reproducibility of AFM measures, Chem. Phys. Lipids. 234 (2021) 105011. https://doi.org/10.1016/j.chemphyslip.2020.105011.

[29] D. Pauluk, A.K. Padilha, N.M. Khalil, et al., Chitosan-coated zein nanoparticles for oral delivery of resveratrol: formation, characterization, stability, mucoadhesive properties and antioxidant activity, Food Hydrocolloids 94 (2019) 411-417. https://doi.org/10.1016/j.foodhyd.2019.03.042.

[30] Y. Wang, S. Wang, C.K. Firempong, et al., Enhanced solubility and bioavailability of naringenin via liposomal nanoformulation: preparation and *in vitro* and *in vivo* evaluations, AAPS PharmSciTech 18 (2017) 586-594. https://doi.org/10.1208/s12249-016-0537-8.

[31] M.K. Gupta, J.A. Singh, Cardiovascular disease in gout and the protective effect of treatments including urate-lowering therapy, Drugs 79 (2019) 531-541. https://doi.org/10.1007/s40265-019-01081-5.

[32] H. Wu, Y. Wang, J. Huang, et al., Rutin ameliorates gout via reducing XOD activity, inhibiting ROS production and NLRP3 inflammasome activation in quail, Biomed. Pharmacother. 158 (2023) 114175. https://doi.org/10.1016/j.biopha.2022.114175.

[33] N. Cho, H. Suemizu, H. Kamimura, et al., Formation of reactive metabolites of benzbromarone in humanized-liver mice, Drug Metab. Pharmacokinet. 47 (2022) 100467. https://doi.org/10.1016/j.dmpk.2022.100467.

[34] S. Lemprière, NLRP3 inflammasome activation implicated in tau pathology, Nat. Rev. Neurol. 16 (2020) 4. https://doi.org/10.1038/s41582-019-0299-5.

[35] X. Meng, C. Fryganas, V. Fogliano, et al., Double-coated nanoliposomes improve the bioavailability of flavanone hesperetin, Food Hydrocolloids 151 (2024) 109872. https://doi.org/10.1016/j.foodhyd.2024.109872.

[36] S. Liu, J. Lian, Z. Xu, et al., Chitosan-coated nanoliposomes for efficient delivery of betanin with enhanced stability and bioavailability, Food Hydrocolloids 132 (2022) 107871. https://doi.org/10.1016/j.foodhyd.2022.107871.

[37] A. Banerjee, J. Qi, R. Gogoi, et al., Role of nanoparticle size, shape and surface chemistry in oral drug delivery, J. Control. Release 238 (2016) 176-185. https://doi.org/10.1016/j.jconrel.2016.07.051.

[38] R.A. Demel, B. de Kruyff, The function of sterols in membranes, Biochim. Biophys. Acta. 457 (1976) 109-132. https://doi.org/10.1016/0304-4157(76)90008-3.

[39] K. Tai, F. Liu, X. He, et al., The effect of sterol derivatives on properties of soybean and egg yolk lecithin liposomes: stability, structure and membrane characteristics, Food Res. Int. 109 (2018) 24-34. https://doi.org/10.1016/j.foodres.2018.04.014.

[40] S. Wu, G. Liu, P. Shao, et al., Transdermal sustained release properties and anti-photoaging efficacy of liposome-thermosensitive hydrogel system, Adv. Healthc. Mater. 13 (2024) 2301933. https://doi.org/10.1002/adhm.202301933.

[41] C. Chen, X. Jie, Y. Ou, et al., Nanoliposome improves inhibitory effects of naringenin on nonalcoholic fatty liver disease in mice, Nanomedicine 12 (2017) 1791-1800. https://doi.org/10.2217/nnm-2017-0119.

[42] S. Jiang, F. Ma, J. Lou, et al., Naringenin reduces oxidative stress and necroptosis, apoptosis, and pyroptosis in random-pattern skin flaps by enhancing autophagy, Eur. J. Pharmacol. 970 (2024) 176455. https://doi.org/10.1016/j.ejphar.2024.176455.

[43] M. Yu, L. Xu, F. Tian, et al., Rapid transport of deformation-tuned nanoparticles across biological hydrogels and cellular barriers, Nat. Commun. 9 (2018) 2607. https://doi.org/10.1038/s41467-018-05061-3.

[44] Y. Zheng, L. Xing, L. Chen, et al., Tailored elasticity combined with biomimetic surface promotes nanoparticle transcytosis to overcome mucosal epithelial barrier, Biomaterials 262 (2020) 120323. https://doi.org/10.1016/j.biomaterials.2020.120323.

[45] Y. Chen, Z. Guo, H. Chen, et al., Salinomycin, a potent inhibitor of XOD and URAT1, ameliorates hyperuricemic nephropathy by activating NRF2, modulating the gut microbiota, and promoting SCFA production, Chem. Biol. Interact. 403(1) (2024) 111220. https://doi.org/10.1016/j.cbi.2024.111220.

[46] S. Gong, J. Chen, X. Zheng, et al., Kidney targeting and modulating macrophage polarization through AMPK signaling: therapeutic mechanism of berberine in uric acid nephropathy, Int. Immunopharmacol. 138 (2024) 112632. https://doi.org/10.1016/j.intimp.2024.112632.

[47] W.A. Verri, T.M. Cunha, C.A. Parada, et al., Hypernociceptive role of cytokines and chemokines: targets for analgesic drug development? Pharmacol. Ther. 112 (2006) 116-138. https://doi.org/10.1016/j.pharmthera.2006.04.001.

[48] N. Kelley, D. Jeltema, Y. Duan, et al., The NLRP3 inflammasome: an overview of mechanisms of activation and regulation, Int. J. Mol. Sci. 20 (2019) 3328. https://doi.org/10.3390/ijms20133328.

[49] S. Fenyk, C. Dixon, W. Gittens, et al, The tomato nucleotide-binding leucine-rich repeat (NLR) immune receptor I-2 couples DNA-binding to nucleotide-binding domain nucleotide exchange, J. Biol. Chem. 291 (2015) 698589. https://doi.org/10.1074/jbc.M115.698589.

[50] C. Ising, C. Venegas, S. Zhang, et al., NLRP3 inflammasome activation drives tau pathology, Nature 575 (2019) 669-673. https://doi.org/10.1038/s41586-019-1769-z.